

Improved Drive-Current into Nanoscaled Channels using Electrostatic Lenses

P. Ellinghaus, M. Nedjalkov, and S. Selberherr

Institute for Microelectronics, TU Wien, Gußhausstraße 27–29/E360, 1040 Wien, Austria

E-mail: {ellinghaus | nedjalkov | selberherr}@iue.tuwien.ac.at

Abstract—The contact regions in nanoscaled transistors play an increasingly important role in the overall performance of the devices. An electrostatic lens in the source contact region to focus a beam of electron wave packets into a nanoscaled channel is investigated here, using a Wigner Ensemble Monte Carlo simulator. An improvement in the drive-current is achieved by reducing reflections from the surrounding oxide. The associated modifications to the momentum distributions are readily shown by using the phase space description of the Wigner formalism.

I. INTRODUCTION

The dimensions of the channel in modern transistor architectures, like multigate-FETs or UTB-SOI, have progressively been scaled down to retain adequate electrostatic control of the channel. The connecting source/drain extensions, however, remain relatively large and have started to play a significant role in the overall performance of the device [1]. Therefore, considerations are made to optimize these regions, e.g. to reduce the contact and access resistances [2]. We investigate the use of an electrostatic lens in the source region to increase the drive-current through the channel by focusing the electrons into the channel aperture and thereby reducing reflections from the adjacent oxide.

An electrostatic lens refers to a specially shaped potential with convex/concave features, similar to optical lenses, used to steer coherent electrons. The concept was first demonstrated experimentally in 1990 in [3], [4], in low-temperature, high-mobility semiconductors, which ensured that the coherent electrons had a sufficiently long mean free path to conduct experiments with structures made with the lithographic capabilities at the time. The astounding decrease of the feature sizes in semiconductor devices, along with novel materials like graphene, has made (semi-)ballistic electron transport applicable at room temperature [5]. This has sparked new interest in applying electrostatic lenses in nanoelectronic devices, e.g. [6] suggests the use of lenses to focus electrons to the center of nanowires, thereby avoiding rough interfaces and increasing mobility.

II. ELECTROSTATIC LENSES

Electrostatic lenses use analogous concepts from geometrical optics: Snell's law describes the refraction of a light beam traversing an interface between two different media of propagation, e.g. air and glass. An equivalent law of refraction can be derived for electrostatic lenses using the principle of energy conservation: A particle with a wavevector \mathbf{k} has a kinetic energy

$$E_k = \frac{\hbar^2 |\mathbf{k}|^2}{2m^*}, \quad (1)$$

where \hbar denotes the reduced Planck constant and m^* the effective mass. As a particle traverses the interface between regions at different potentials (illustrated in Fig. 1), its kinetic and potential energies change. The change in kinetic energy is attributed only to the change of the component of the wave vector normal to the interface (red); the component parallel to the interface (blue) is left unchanged. It follows that

$$|\mathbf{k}_1| \sin \theta_1 = |\mathbf{k}_2| \sin \theta_2, \quad (2)$$

where θ_1 (θ_2) is the angle of incidence (refraction) with respect to the normal of the interface. The magnitude of the wave vector is proportional to the square root of the kinetic energy:

$$\frac{\sin \theta_2}{\sin \theta_1} = \frac{|\mathbf{k}_1|}{|\mathbf{k}_2|} = \frac{\sqrt{E_{k_1}}}{\sqrt{E_{k_2}}}. \quad (3)$$

Therefore, the square root of the kinetic energy of a particle is analogous to the refractive index used in geometrical optics and this value can be dynamically modified by changing the value of the potential in the region of the lens. A larger value of the potential for the lens (relative to its surrounding region) invokes a stronger refraction ('bending'). However, since the lens also acts as a potential barrier (assuming a positive value) the degree of reflection also increases – a trade-off must be found. If a positive potential step is used for the lens, the kinetic energy (refractive index) decreases and the electron is bent away from the normal to the interface. This dictates that a double-concave shape is needed to form a converging lens with a positive potential [4]. Fig. 2 shows an example of a wave packet which is focused when traveling through a double-concave converging lens.

A further consideration for designing the lens is that the size of the lens should be larger than the de Broglie wavelength of the electron (determined by its energy), otherwise an effective focusing will be distorted by diffraction effects.

III. SIMULATION SETUP

A. Simulator

The Wigner formalism describes quantum physics in the phase space in terms of functions and variables and is convenient to investigate transient and stationary processes in multi-dimensional semiconductor structures, ranging from quantum-coherent to scattering-dominated transport. The simulation results presented here were obtained using the Wigner Ensemble Monte Carlo (WEMC) simulator included in ViennaWD [7]. This simulator has been shown to provide highly accurate results for the coherent evolution of wave packets [8].

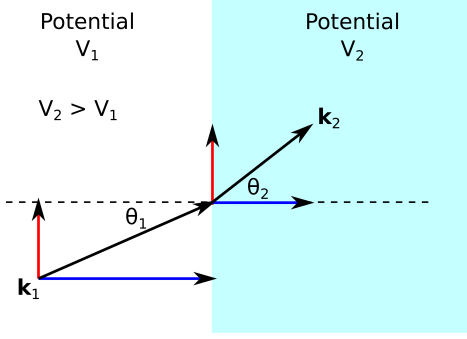


Figure 1: The wave vector of a particle is changed from \mathbf{k}_1 to \mathbf{k}_2 as the interface between regions at different potentials is traversed. The decomposition of each wave vector into its components normal (blue) and parallel (red) to an interface is shown. The normal component is modified according to the potential change, whereas the parallel component remains unchanged. The illustrated case assumes a positive potential step, where $V_2 > V_1$, such that the particle is refracted away from the normal to the interface.

The semi-discrete Wigner equation considers a finite coherence length (L), which discretizes the k -space with a resolution of $\Delta k = \frac{\pi}{L}$, and is given by

$$\frac{\partial f_w}{\partial t} + \frac{\hbar q \Delta k}{m^*} \frac{\partial f_w}{\partial x} = \sum_{q=-K}^K V_w(x, q - q', t) f_w(x, q', t), \quad (4)$$

where q is an index which refers to the quantized momentum, i.e. $p = \hbar(q\Delta k)$. The Wigner potential is akin to a Fourier transform of the potential differences within the coherence length around a point and is defined as

$$V_w(x, q) \equiv \frac{1}{i\hbar L} \int_{-L/2}^{L/2} ds e^{-i2q\Delta k \cdot s} \delta V(s; x); \quad (5)$$

$$\delta V(s; x) \equiv V(x + s) - V(x - s).$$

The WEMC simulator uses the signed-particle method [9] to solve (4) by generating numerical particles in pairs with $+$ and $-$ signs, which capture the quantum information. The statistics for the particle generation (rate and momentum offsets) are dictated by the Wigner potential (5). The Wigner potential encapsulates higher-order derivatives of the potential and not only its first derivative, i.e. electric field, as in the classical Boltzmann equation.

B. Geometry

The geometry considered for the simulations is shown in Fig. 3. This geometry is representative for many current transistor structures where a narrow channel (< 10 nm) is surrounded/sandwiched by oxide and is extended to a larger drain/source contact region; the drain region is not shown. The oxide is approximated by a 0.4 eV potential barrier, which is sufficient to constrain the wave packets to the channel and source regions without inducing excessive particle generation

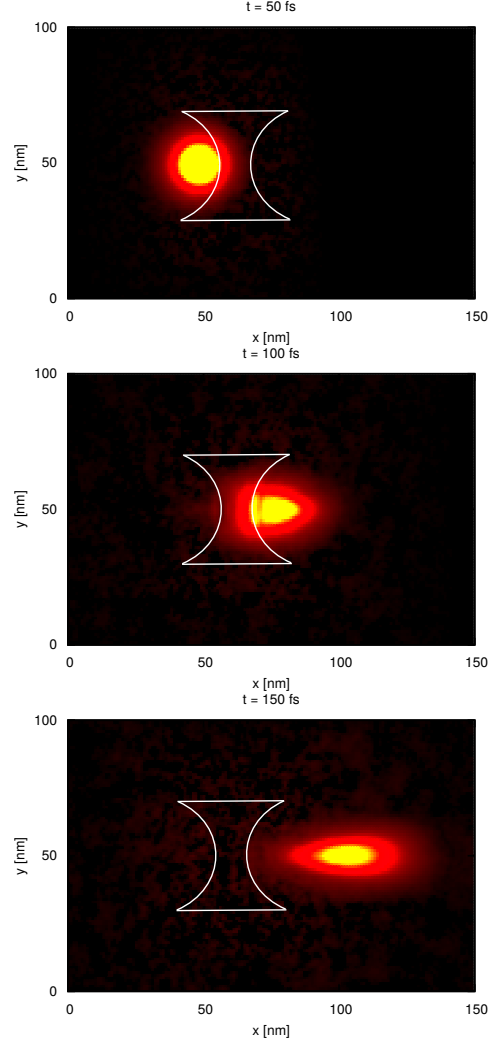


Figure 2: The density of a Gaussian wave packet, over a sequence of time steps, is focused by a converging electrostatic lens with a double-concave shape (as indicated by the annotation in white). The wave packet has a kinetic energy of 180 meV and the lens has a potential of 40 meV.

(the generation rate is related to the magnitude of the potential differences). Wave packets are periodically injected from the left boundary towards the channel. A converging electrostatic lens is placed before the aperture of the channel to focus the wave packets into the channel. The de Broglie wavelength of the wave packets considered here is in the order of a few nanometers, which requires the lens to be at least 10 nm wide to avoid diffraction effects.

C. Steady-state Current

The WEMC simulator is utilized here to calculate the steady-state current through the channel, by the periodic injection of minimum uncertainty wave packets from the left contact (boundary) in Fig. 3. Each wave packet represents a

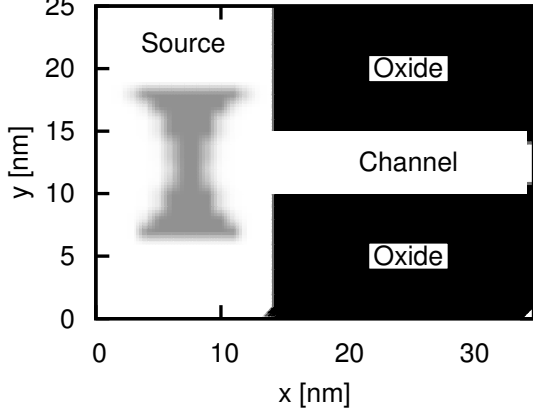


Figure 3: A 5 nm wide channel sandwiched between two oxide layers (black) with an adjacent source region with a double-concave lens (gray), at 40 meV, positioned in front of the aperture to the channel. The left and right boundaries of the shown domain are considered as contacts (absorbing/emitting particles), whereas reflecting boundary conditions are imposed on the top and bottom boundaries. Wave packets are injected from the left 'contact' periodically every 10 fs.

Table I: Simulation parameters

σ [nm]	L_{coh} [nm]	Δk [nm ⁻¹]	\mathbf{k}_0 [nm ⁻¹]	\mathbf{x}_0 [nm]
3 ÷ 5	30	π/L_{coh}	$(9\Delta k, 0)$	$(\cdot, 12.5)$

single electron and is defined by

$$f_w(\mathbf{x}, \mathbf{q}) = \mathcal{N} e^{-\frac{(\mathbf{x}-\mathbf{x}_0)^2}{\sigma^2}} e^{-(\mathbf{q}\Delta k - \mathbf{k}_0)^2 \sigma^2}, \quad (6)$$

where \mathbf{x}_0 and \mathbf{k}_0 are two-dimensional vector quantities representing the mean position and the mean wavevector, respectively; σ is the standard spatial deviation and \mathcal{N} represents a normalization constant. The wave packet travels in the two-dimensional plane towards the right (x -direction). A distribution function, e.g. Maxwell-Boltzmann, can be sampled to select the energy (wave vector) of each wave packet injected from the source contact; here, we inject identical wave packets, with the parameters defined in Table I, which corresponds to a mean energy of approximately 200 meV. The magnitude of the injected current is set by the value of the period of injection T_{inj} , i.e.

$$I = \frac{q}{T_{inj}}. \quad (7)$$

The drive-current (through the channel) is calculated by the Ramo-Shockley theorem [10], adapted to account for the signed numerical particles used in the WEMC simulator:

$$I = -\frac{1}{L_x} \frac{e}{N_{wp}} \sum s_i v_i, \quad (8)$$

where L_x , N_{wp} , and e represent the device length in the x -direction (35 nm), the number of numerical particles representing one injected wave packet and the unit charge, respectively. The summation is performed over the entire particle ensemble, taking the sign (s_i) and the x -velocity (v_i) of each numerical particle into account. The electric field is assumed to be uniform across the channel, directed rightwards, i.e. $\mathbf{E} = (0, E_x)$.

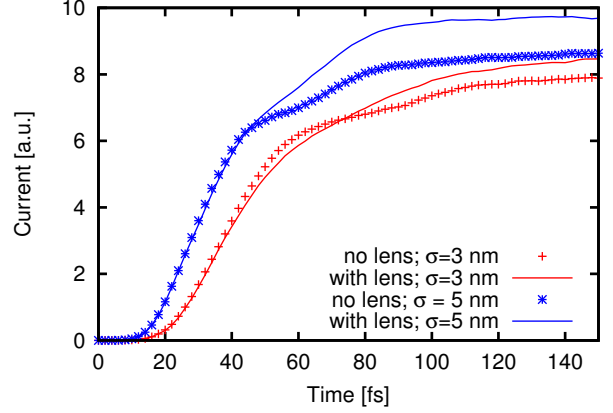


Figure 4: Comparison of the channel currents achieved with and without the addition of a 40 meV electrostatic lens for wave packets with a spatial standard deviation of 3 nm and 5 nm.

IV. RESULTS

Simulations, using the geometry in Fig. 3, are run with and without the addition of a converging lens in front of the aperture to the transistor channel. The steady-state current is calculated for wave packets with a standard deviation of 3 nm and 5 nm, as shown in Fig. 4. The addition of the lens consistently increases the drive current; the gains made by focusing the wave packets into the channel are larger than the losses from reflections by the lens, which presents a small potential barrier to the electrons. The lens shows a better effect, when a (spatially) broader wave packet is focused and increases the channel current by 15% if $\sigma = 5$ nm, compared to an 8% increase if $\sigma = 3$ nm. Some uncertainty exists about the true value of the standard deviation for the wave packet [11]. Moreover, the Gaussian wave packet spreads out as it propagates. The current gradually rises as the domain is filled with particles before it converges to a steady-state value after approximately 140 fs.

Fig. 5 compares the evolution of the probability density towards a steady state with and without a lens. Due to the focusing of the wave packets by the lens, the reflections from the oxide barriers next to the aperture of the channel are reduced. This observation is supported by the associated difference of the k_x -distributions. Fig. 6 (a) shows the change in k_x -distributions corresponding to Fig. 5 (a); the reduction in the kinetic energy of the wave packets due to the potential barrier presented by the lens is clearly shown. However, once the steady-state is reached (at approximately $t = 140$ fs; Fig. 6 (b)) a reduction in the probability of left-moving (negative k_x) particles is observed, indicating the lens leads to reduced reflections overall; the forward-moving particles (around $5\Delta k$) are enhanced.

V. CONCLUSION

In conclusion, the addition of a converging electrostatic lens in the source region of a transistor can be used to effectively focus electron wave packets into a nanoscale channel by reducing reflections from the oxide surrounding the

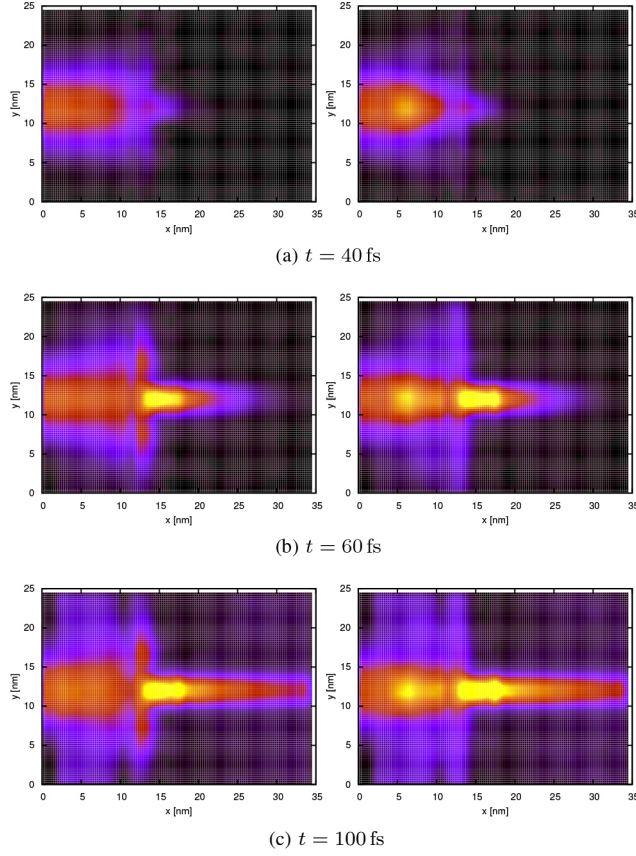


Figure 5: Comparison of the evolution of the particle density for the structure in Fig. 1 without (left) and with (right) a lens. A wave packet with $\sigma = 5$ nm is injected every 10 fs. The density at the sides of the aperture to the channel is reduced by the addition of the lens.

aperture. Moreover, the results illustrate for the first time how a steady-state current is obtained with a two-dimensional WEMC simulator, allowing it to be applied to investigate practical issues of semiconductor devices.

REFERENCES

- [1] A. Dixit, A. Kottantharayil, N. Collaert, M. Goodwin, M. Jurczak, and K. De Meyer, "Analysis of the Parasitic S/D Resistance in Multiple-Gate FETs," *Electron Devices, IEEE Transactions on*, vol. 52, pp. 1132–1140, June 2005.
- [2] A. Villalon, C. Le Royer, S. Cristoloveanu, M. Casse, D. Cooper, J. Mazurier, B. Previtali, C. Tabone, P. Perreau, J.-M. Hartmann, P. Scheiblin, F. Allain, F. Andrieu, O. Weber, and O. Faynot, "High-Performance Ultrathin Body c-SiGe Channel FDSOI pMOSFETs Featuring SiGe Source and Drain: V_{th} Tuning, Variability, Access Resistance, and Mobility Issues," *Electron Devices, IEEE Transactions on*, vol. 60, pp. 1568–1574, May 2013.
- [3] U. Sivan, M. Heiblum, C. P. Umbach, and H. Shtrikman, "Electrostatic Electron Lens in the Ballistic Regime," *Phys. Rev. B*, vol. 41, pp. 7937–7940, Apr 1990.
- [4] J. Spector, H. L. Stormer, K. W. Baldwin, L. N. Pfeiffer, and K. W. West, "Electron Focusing in Two-dimensional Systems by Means of an Electrostatic Lens," *Applied Physics Letters*, vol. 56, no. 13, pp. 1290–1292, 1990.

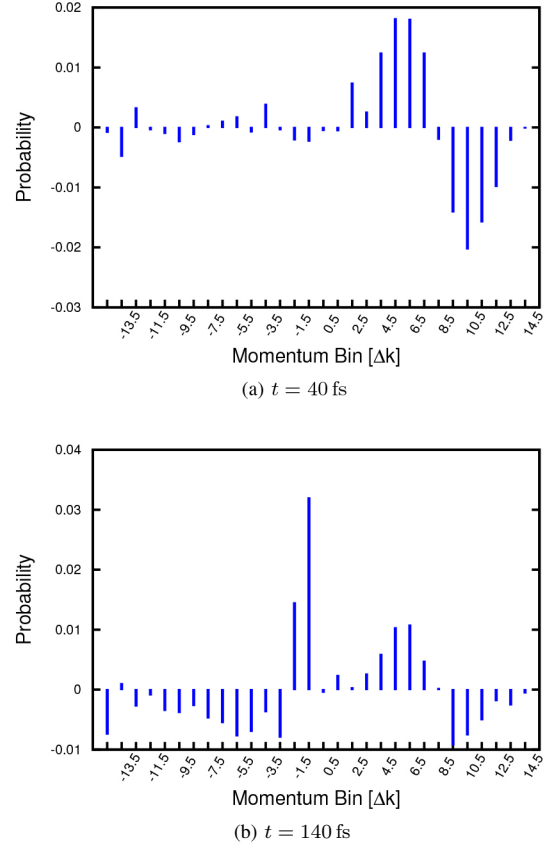


Figure 6: Difference in k_x distributions with and without the addition of a lens after (a) 40 fs and (b) 140 fs of evolution. A positive value indicates components enhanced by the lens; negative values indicate a suppression. The initial reduction in the kinetic energy of the wave packet is seen in (a). Once steady-state is reached (b), an overall reduction in the negative k_x (i.e. leftwards moving) components is evident.

- [5] R. Wang, H. Liu, R. Huang, J. Zhuge, L. Zhang, D.-W. Kim, X. Zhang, D. Park, and Y. Wang, "Experimental Investigations on Carrier Transport in Si Nanowire Transistors: Ballistic Efficiency and Apparent Mobility," *Electron Devices, IEEE Transactions on*, vol. 55, pp. 2960–2967, Nov 2008.
- [6] M. Muraguchi and T. Endoh, "Size Dependence of Electrostatic Lens Effect in Vertical MOSFETs," *Japanese Journal of Applied Physics*, vol. 53, no. 4S, p. 04EJ09, 2014.
- [7] "ViennaWD: Wigner Ensemble Monte Carlo Simulator." <http://viennawd.sourceforge.net/>.
- [8] P. Ellinghaus, M. Nedjalkov, and S. Selberherr, "The Wigner Monte Carlo Method for Accurate Semiconductor Device Simulation," in *Proceedings of the 19th International Conference on Simulation of Semiconductor Processes and Devices (SISPAD)*, pp. 113–116, 2014.
- [9] M. Nedjalkov, P. Schwaha, S. Selberherr, J. M. Sellier, and D. Vasileksa, "Wigner Quasi-Particle Attributes - An Asymptotic Perspective," *Applied Physics Letters*, vol. 102, no. 16, pp. 163113.1–163113.4, 2013.
- [10] H. Kim, H. Min, T. Tang, and Y. Park, "An Extended Proof of the Ramo-Shockley Theorem," *Solid-State Electronics*, vol. 34, no. 11, pp. 1251–1253, 1991.
- [11] D. Ferry, S. Ramey, L. Shifren, and R. Akis, "The Effective Potential in Device Modeling: The Good, the Bad and the Ugly," *Journal of Computational Electronics*, vol. 1, no. 1-2, pp. 59–65, 2002.